Gaseous alkali interactions with ilmenite, manganese oxide and calcium manganite under chemical looping combustion conditions

Fuel Processing Technology 254 (2024) 108029

Contents lists available at ScienceDirect

Fuel Processing Technology

journal homepage: www.elsevier.com/locate/fuproc

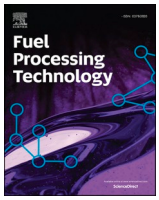

Research article

Gaseous alkali interactions with ilmenite, manganese oxide and calcium manganite under chemical looping combustion conditions

Viktor Andersson [a], Xiangrui Kong [a], Henrik Leion [c], Tobias Mattisson [b], Jan B.C. Pettersson [a,*]

[a] Department of Chemistry and Molecular Biology, Atmospheric Science, University of Gothenburg, Medicinaregatan 7B, SE-413 90 Gothenburg, Sweden
[b] Department of Space, Earth and Environment, Division of Energy Technology, Chalmers University of Technology, Hörsalsvägen 7A, SE-412 96 Gothenburg, Sweden
[c] Energy and Materials, Chemistry and Chemical Engineering, Chalmers University of Technology, Kemigården 4, SE-412 96 Gothenburg, Sweden

ARTICLE INFO

Keywords:
Oxygen carriers
Chemical looping combustion
Alkali
Ilmenite
Manganese oxide
Calcium manganite

ABSTRACT

Alkali species present in biomass pose significant challenges in chemical looping combustion (CLC) processes and other thermal conversion applications. The interactions between different alkali species and three common oxygen carrier (OC) materials that are considered to be state of the art in CLC applications have been investigated. A dedicated fluidized bed laboratory reactor was used to study interactions of KCl, NaCl, KOH, NaOH, K_2SO_4 and Na_2SO_4 with manganese oxide, calcium manganite and ilmenite. Alkali vapor was generated by injecting alkali salts under reducing, oxidizing and inert conditions at 900 °C. Gaseous species were measured online downstream of the reactor, and the efficiency of alkali uptake was determined under different conditions. The result show significant alkali uptake by all OCs under the studied conditions. Ilmenite shows near complete alkali uptake in reducing conditions, while manganese oxide and calcium manganite exhibited less effective alkali uptake, but have advantages in terms of fuel conversion and oxidizing efficiency. Alkali chlorides, sulfates and hydroxides show distinctly different behavior, with alkali hydroxides being efficiently captured all three investigate OC materials. The findings contribute to a deeper understanding of alkali behavior and offer valuable guidance for the design and optimization of CLC with biomass.

1. Introduction

The increasing interest in biomass as a sustainable energy source has prompted the development of efficient biomass thermal conversion technologies. Chemical looping combustion (CLC) has emerged as a promising technology for clean and efficient biomass conversion [1,2]. The CLC process generally involves two interconnected fluidized bed reactors: one fuel reactor where the fuel, e.g., biomass, is introduced and the product gases consist mainly of carbon dioxide and steam, and one air reactor where air is introduced and the flue gases consist mainly of oxygen depleted air [3]. In contrast to conventional combustion processes where air is used as oxidizer to burn the fuel, CLC utilize a solid material called an oxygen carrier (OC) to transfer oxygen from the air to the fuel. The OC, typically a metal oxide, is oxidized in the exothermic air reactor and transported through a loop-seal to the reducing fuel reactor where it releases oxygen to facilitate the fuel conversion, before being transported back to the air reactor to complete the circulation [4]. The key advantage of CLC is that it inherently separates carbon dioxide from nitrogen in the air during the combustion process [3]. The CO_2 is concentrated and easily captured from the fuel reactor, while the nitrogen is not involved in the combustion reactions and exits the system separately. This makes carbon capture and storage (CCS) economically viable and energy-efficient, which may result in negative CO_2 emissions if biomass is used as fuel source [2]. Chemical looping combustion thus has the potential to significantly reduce CO_2 emissions while maintaining high energy efficiency in various industries, including power generation and industrial processes. However, like other emerging technologies, it faces challenges in terms of scale-up, cost-effectiveness, and system optimization.

One of the major challenges encountered in CLC of biomass is the presence of alkali species, predominantly derived from the biomass feedstock. Alkali, primarily in the form of Na and K compounds, can cause operational issues such as high-temperature corrosion and fouling of heat transfer surfaces, or affect the performance of fluidized bed materials [5–10]. In CLC systems, alkali is introduced into the fuel reactor along with the biomass fuel. During fuel conversion, it can be expected that a fraction of the alkali is released into the gas phase, where it can either react with the OC or leave the reactor with the flue gases.

* Corresponding author.
E-mail address: janp@chem.gu.se (J.B.C. Pettersson).

https://doi.org/10.1016/j.fuproc.2023.108029
Received 7 November 2023; Received in revised form 20 December 2023; Accepted 27 December 2023
Available online 6 January 2024

Most of the heat extraction occurs after the air reactor of a CLC process. To prevent detrimental fouling and corrosion of superheater tubes [11,12], it is important to limit the gaseous alkali emissions in the oxidizing atmosphere. Therefore, it is likely more beneficial to have high alkali concentrations in the flue gases leaving the fuel reactor or to let the alkali be absorbed by the bed material. If the alkali is taken up by the OC, it may influence its overall performance and lead to operational challenges or potential degradation risks [7,8,13]. One known issue is melted phases that forms when alkali reacts with silica, causing the OC particles to agglomerate and possibly defluidize the bed [14–17]. It is also possible that the alkali might influence OCs reactivity, oxygen transfer capabilities or life time [18]. Alkali metals also exhibit catalytic effects in various reactions, including carbon conversion, tar cracking, and char reactivity [19–22]. Several studies have shown that increasing the potassium content in biomass enhances gasification reactivity and a high K/C ratio increases the gasification rate during CO_2 gasification [23–27]. Understanding the behavior of alkali species and their interaction with OC materials are consequently vital for optimizing CLC processes and minimizing alkali-related issues.

Another crucial aspect to consider when optimizing a CLC process is the choice of OC material. Various materials have been studied, including metal oxides, mixed metal oxides, and perovskite-type compounds, and the selection depends on several factors, such as reactivity, chemical and mechanical stability, toxicity, cost and availability [4]. The choice of OC for a certain CLC application is based on the chemical and physical properties of the material, including factors like reactivity, oxygen transfer efficiency and material degradation. This study focuses on three different OCs: calcium manganite ($CaMnO_3$), manganese oxide (Mn_3O_4), and ilmenite ($FeTiO_3$). The OC materials were chosen for this study since they are currently considered state of the art in the CLC community. They are, however, highly suitable for other conversion applications as well [28–31]. The first two are examples of synthetic materials which generally consist of monometallic or combined oxides [32,33], which are often considered expensive with the benefit of reaching high fuel conversion rates [34]. In comparison, ilmenite is an example of a naturally occurring mineral which is less costly with the drawback of a lower fuel conversion efficiency. Other examples of natural materials for thermal conversion processes are manganese [35,36] and iron ores [37].

Calcium manganite has mostly been studied in CLC with gaseous fuels, although some studies with solid biomass have been reported [5]. The material has demonstrated excellent performance, achieving high fuel conversion rates [34] and exhibiting a prolonged operational lifetime [38]. It has an advantage over previously used OCs like nickel oxides, as it can be produced from low-cost materials, does not have the health and safety issues associated with nickel, and can release oxygen to the gas phase [5,39]. However, calcium manganite may not be suitable for ash-rich solid fuels like coal due to potential OC losses in ash streams and its sensitivity to sulfur [34]. Calcium manganite shows promise for low-ash and low-sulfur fuels, such as biomass, with pilot studies indicating high conversion rates and OC particle life time comparable to nickel oxides [5]. Furthermore, calcium manganite have the ability to release gaseous oxygen in the FR. The phenomena is called chemical-looping with oxygen uncoupling (CLOU) [40]. This leads to enhanced fuel conversion and increased overall system efficiency, especially for solid fuels, since it allows for direct reaction between the solid fuel and gaseous oxygen [41,42]. Conversion of solid fuels by OC without CLOU properties requires the fuel to be gasified with e.g., steam or CO_2 before the reaction between the resulting fuel gas and solid OC [43]. Therefore, the conversion rate for solid fuels is higher when using OC with CLOU properties, since the slow process of fuel gasification can be avoided.

Other highly interesting materials for CLC that possess CLOU properties are manganese-based OCs. Several studies have investigated the use of manganese ores [43–45] and synthetically manufactured manganese-based oxides, often supported on inert stabilizers such as zirconia [46,47]. Manganese-based OCs are regarded as interesting materials for biomass thermal conversion systems, such as CLC, for several compelling reasons. Manganese oxide is not toxic and its thermodynamic properties allow for recurring oxidation and reduction in conditions relevant for thermal conversion applications [44]. The materials possess high thermal stability and regenerability which are crucial for maintaining their structural integrity and performance without significant loss of reactivity during continuous CLC operation [46]. In addition, manganese ores are abundant in various regions worldwide and are considered a cost-effective option for large-scale applications.

Ilmenite, an iron-titanium oxide mineral ($FeTiO_3$), has also emerged as a promising OC material due to its attractive properties and is now considered one of the most scrutinized OC materials [48,49]. Ilmenite is a robust and durable OC material that possesses high oxygen-carrying capacity, good chemical stability and low cost, making it a viable alternative to other OC materials [28,50–52]. Ilmenite is abundant in various geological deposits worldwide, which ensures a reliable and sustainable supply. Previous ilmenite studies investigating the interactions with biomass ash components show effective uptake of potassium [51,53] forming potassium titanates, $KTi_8O_{16.5}$ [6]. In addition, the alkali uptake does not seem to cause particle agglomeration [6,51], which is why the material may be used as an alkali scavenger in CLC, decreasing the gaseous alkali emissions.

While some studies have investigated the interactions between alkali metals and ilmenite, similar investigations on manganese oxide and calcium manganite are scarce. In addition, most of the alkali-related studies available in the literature are based on off-line characterization of material from industrial processes and related to solid-solid interactions between ash and OC [6,28,51]. It is expected that significant fractions of alkali will be released in conjunction with the devolatilization of the biomass. Thus, significant fractions of the alkali will likely be in the gas phase surrounding the OC bed material, and gas-solid reactions are expected to be highly important, but not studied to a large extent in the literature. Building on previous research, which has primarily focused on designing a suitable reactor system and the interactions between alkali and a specific OC [54–56], this study presents an investigation into the behavior of alkali species in biomass thermal conversion systems using different OC materials and their implications for CLC systems. The study includes investigations of the interaction between six alkali metal compounds (KCl, KOH, K_2SO_4, NaCl, NaOH and Na_2SO_4) and three different OC materials, to provide insights into some of the complex gas-solid interactions taking place within a CLC process.

2. Experimental methodology

The experimental studies involve a fluidized bed reactor system capable of simulating the complex fluid dynamics and gas-solid interactions encountered in practical CLC applications [56]. The experimental setup schematically shown in Fig. 1 utilizes a laboratory-scale fluidized bed reactor made of Kanthal APMT™ steel with excellent corrosion resistance, operating at 900 °C under recurring oxidizing, inert and reducing conditions. A perforated plate of stainless steel alloy 316 is used as gas distributor and particle filter for the OC material, which is fluidized during continuous injection of an alkali salt. The reactor has been described in detail elsewhere [56], and is externally heated by an electric furnace enabling precise temperature control during the experiments. A modification compared to the previous description of the setup [56], is the employment of heating cords on the exhaust lines. Alkali salt aerosol and reactor gases are introduced to the fluidized bed with adjustable and stable concentrations. The concentrations of gases and alkali are monitored on-line in the reactor exhaust, which provides valuable insights into the interactions between alkali compounds and OC particles under different conditions. The pressure difference between the top and bottom of the reactor and the reactor temperature are continuously monitored to ensure proper fluidization

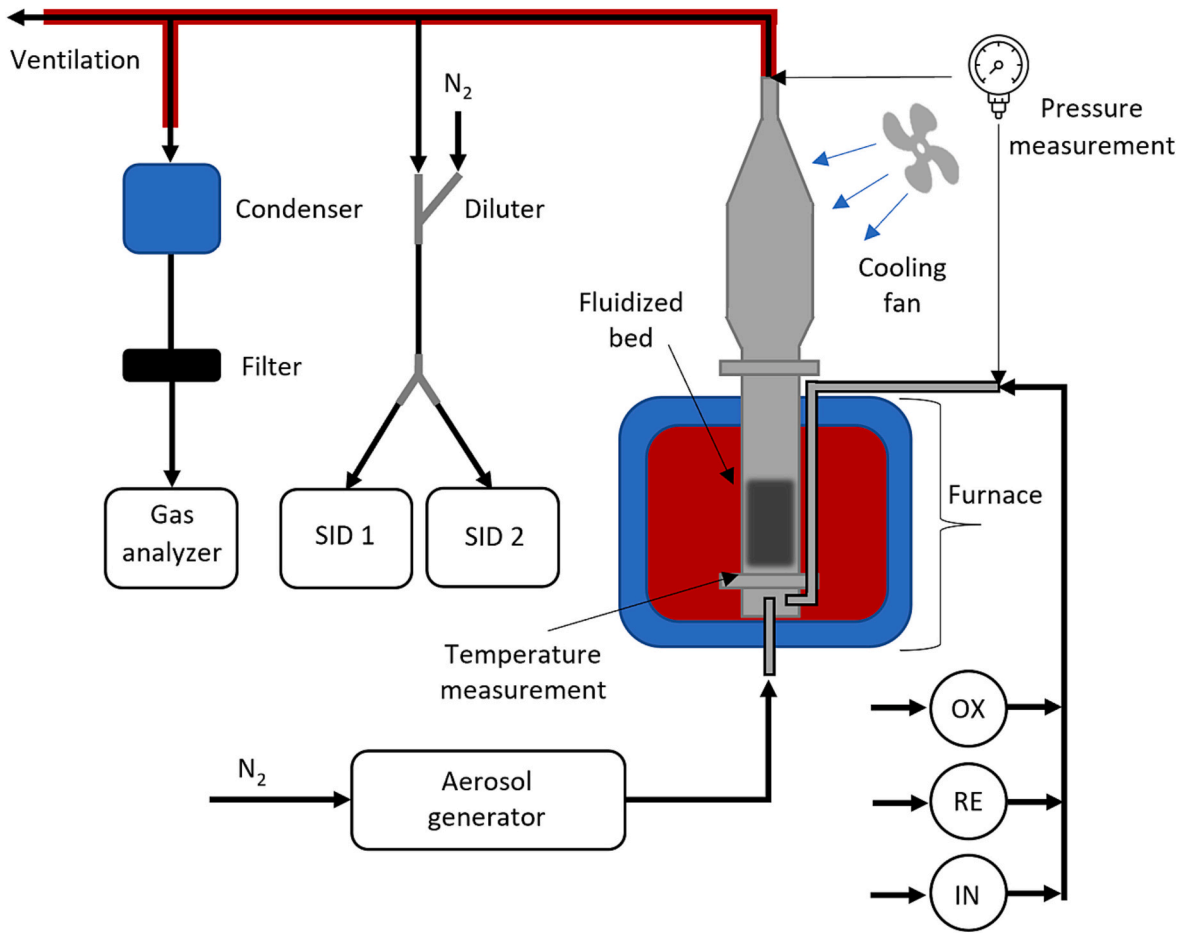

Fig. 1. Schematic illustration of experimental setup including the laboratory-scale reactor that is externally heated by an electric furnace. Alkali aerosol is generated using an aerosol atomizer, and the produced aerosol is fed through a tube with 6 mm diameter at the bottom of the reactor. An automated valve system regulates the flow of oxidizing (OX), reducing (RE) and inert (IN) gases, which are preheated along the reactor body before being introduced at the bottom of the reactor. A fan provides additional cooling to the topmost section of the reactor. Heating cords (marked in red) are used to prevent water condensation and subsequent flow disturbances in the exhaust lines. The outlet gases are fed to two alkali detectors (SID1 and SID2) and a gas analyzer. (For interpretation of the references to colour in this figure legend, the reader is referred to the web version of this article.)

and operating temperature of the fluidized bed. The temperature decreases rapidly in the unheated and uninsulated upper part of the reactor, which results in efficient formation of alkali aerosol particles by nucleation [56]. These aerosol particles are subsequently transported with minimal losses to downstream detectors [56].

A stable and controllable alkali aerosol particle generation process is crucial for the experimental procedure. To introduce the alkali, submicron aerosol particles dispersed in a 1 L min^{-1} nitrogen flow were generated by an aerosol generator (Model 3076, TSI Inc.) and fed from the bottom of the reactor. The aerosol particles were generated by dissolving KCl, KOH, K_2SO_4, NaCl, NaOH or Na_2SO_4 in ultrapure water, resulting in a 0.05 M salt solution that was atomized with nitrogen. After atomization, the polydisperse wet aerosol particles are dried in a silica diffusion dryer. A detailed description of the alkali aerosol generation process is available in a previous publication [54]. Before entering the fluidized bed reactor, the 1 L min^{-1} aerosol flow was mixed with 0.5 L min^{-1} of reactor gases to replicate the inert, reducing, and oxidizing environments of a chemical looping combustion system. The reactor gases included N_2 mixed with synthetic fuel gas (50% H_2 in CO), or synthetic air (21% O_2 in N_2), which led to a concentration of approximately 20 mg m^{-3} (KCl or NaCl) or 40 mg m^{-3} (KOH, NaOH, K_2SO_4 or Na_2SO_4) alkali aerosol in 1.5 L min^{-1} of either pure N_2, 10 vol% H_2 and 10 vol% CO in N_2, or 7 vol% O_2 in N_2 following the gas mixing step. The alkali concentrations are comparable to the typical range of alkali concentrations measured during CLC of biomass (1–35 mg m^{-3}) [5]. The alkali aerosol concentration was measured by a scanning mobility particle sizer (Model 3936, TSI Inc.) [54]. The difference in alkali mass concentration is a consequence from using the same concentration of the salt solution for all alkali compounds in the aerosol generation process. An alternative approach would be to adjust the concentration of the salt solution to generate the same mass concentration of aerosol particles for all compounds. However, the measured aerosol mass concentration is greatly influenced by the water content in the aerosols. The water activity of KOH ($a_w = 0.115$) is around five times lower compared to KCl ($a_w = 0.616$) in a saturated salt solution at room temperature, meaning that KOH aerosols are significantly more prone to absorb and hold water from the air compared to KCl [57]. In turn, this affects the aerosol drying process and therefore the measured aerosol mass concentration. This explains the comparably larger mass concentration of hydroxides compared to chlorides, i.e., an overestimation of the mass concentration due to a higher water content in the aerosols. In reality, we assume that the amounts of K and Na being fed to the reactor in the hydroxide experiments are similar to the chloride experiments. However, based on the molar ratio, twice the amount of K and Na are fed to the reactor in the sulphate experiments compared to the chloride and hydroxide experiments.

The conversion of H_2 in reducing conditions forms up to 10 vol% H_2O, or 1.5 g H_2O(l) (assuming all H_2 is converted to 150 NmL min^{-1} H_2O(g) for 800 s) during each reducing stage. Some additional amount of H_2O is expected to be continuously introduced to the reactor system

with the aerosol flow as a result of the alkali generation process. Therefore, heating cords that operate at 130 °C are used to heat the exhaust lines leaving the reactor to prevent condensation of water. After exiting the reactor, the gas is separated into three streams. One stream flows to two alkali detectors, another stream passes through a condenser and particle filter to a gas analyzer, and the remaining gas is directed to a ventilation system. The sample gas for alkali measurements was diluted 10 times with N_2 before entering the instruments. The alkali concentration was measured by two surface ionization detectors (SID) placed in parallel. Each SID measure the alkali concentration in the gas flow using the technique of surface ionization on a hot platinum surface [58,59]. A detailed description of the SID technique has been reported elsewhere [58,60–62] and the instrument has been used in several earlier combustion related studies [5,53–55,61,63,64]. The alkali concentration is registered as a current within the SID, which is then transformed into an alkali mass concentration by a separate calibration method that has been reported in a previous study [62]. One of the two SIDs is operated with a constant platinum surface temperature of 1100 °C and measures the total alkali concentration in the gas flow with 1 s time resolution. The platinum surface temperature of the second SID is periodically shifted between 550, 1100, 800 and 1100 °C with 30 s duration at each temperature. This method has recently been developed to distinguish between potassium and sodium and to enable speciation of the alkali compounds that are present in the gas flow (see Appendix A). A gas analyzer (Model NGA 2000, Emerson Electric Co.) is used to determine the concentrations of O_2, CO_2, CO, H_2, and CH_4 in the gas stream with a time resolution of 2 s.

2.1. Oxygen carriers

Three different types of OCs were used in this study. Two of the materials, one consisting of calcium manganite and one on manganese oxide, were synthetically manufactured, while the third material was a natural ilmenite ore. Prior to the fluidized bed experiments, all OC particles were sieved to fit within the 90–250 μm size range.

The calcium manganite OC was synthetically manufactured with a spray-drying technique from pro-analysis chemicals by the Flemish Institute Technological Research, Belgium. It is a perovskite material with molar composition $CaMn_{0.775}Ti_{0.125}Mg_{0.1}O_{3-\delta}$, where the magnesium occurs in a separate phase, while the other elements bind together in the perovskite structure [65]. The material has been used in previous studies investigating alkali interactions with OC fluidized bed in laboratory reactors [55,56]. Previous scanning electron microscope analysis indicated contamination of the calcium manganite with a minor fraction of ilmenite particles [55].

This study also employed a synthetic manganese-based oxide supported on magnesium stabilized zirconia. The OC was produced by Johansson et al. [47] and consists of 40 mass% Mn_3O_4 and 60 mass% Mg-ZrO_2. The material was selected after previous successful OC tests in a laboratory-scale fluidized bed reactor [47] and in a 300 W continuously operating CLC system [46]. Mg was added to pure zirconia to enhance its stability at high temperatures. Mn_3O_4 serves as the active phase, while Mg-ZrO_2 functions as a porous support, providing a larger surface area for reaction, and as a binder for increasing the mechanical strength and attrition resistance. The particles were prepared using freeze granulation, and further details of the preparation method can be found in the literature [47].

The third OC used in this study consisted of Norwegian rock ilmenite ($FeTiO_3$) (Titania A/S). The main elements are Fe and Ti with low levels of Si and Mg; a complete elemental composition is presented in [28]. The material was calcined at 950 °C for 12 h in oxidizing atmosphere before being crushed and sieved to the desired particle size range. In addition, the material was activated with several cycles of synthetic air and synthetic fuel gas at temperatures 700, 800 and 900 °C before being used in the alkali studies.

2.2. Experimental parameters

The reactor was filled with 40 g of OC material during the fluidized bed experiments. The operating temperature was 900 °C and each alkali salt compound was continuously injected throughout two, three or four recurring redox cycles before the alkali compound was changed. Each experiment involved heating the reactor while fluidizing the OC with N_2, and subsequently introducing alkali chlorides, alkali hydroxides, and finally alkali sulfates during several redox cycles.

Each redox cycle followed a pattern of subsequent reducing, inert, oxidizing and inert conditions to resemble the atmospheric conditions during circulation between different sections of a CLC process. The time durations in each stage depended on the time required for complete reduction or oxidation of each OC material, and are listed in Table 1. For example, initial experiments with $CaMnO_3$ displayed complete fuel conversion in approximately 790 s, after which the concentrations of fuel gases in the exhaust increase rapidly. Therefore, the time duration in reducing conditions was set to 800 s in the $CaMnO_3$ experiments. The redox cycle for the manganese oxide experiments is significantly shorter compared to those for calcium manganite and ilmenite. This is a consequence from the lower oxygen capacity compared to the other two, since merely 40 mass% of the manganese oxide material is active phase.

3. Results

The primary experimental results consist of alkali and gas concentrations as a function of time in the flux leaving the reactor during operation of a fluidized bed at 900 °C. Alkali aerosol particles with an average diameter of approximately 45 nm are injected to the reactor and the alkali chloride (KCl and NaCl) and hydroxide (KOH and NaOH) particles rapidly evaporate at temperatures exceeding approximately 500 °C [54,62,66], while alkali sulphates (K_2SO_4 and Na_2SO_4) evaporate in the 700–800 °C temperature range [66]. All salts thus evaporate well below the operation temperature of the OC fluidized bed. Consequently, the discussed experimental results concern alkali compounds in gaseous form within the reactor, and specifically interactions between these gaseous alkali compounds and the OC particles. Downstream of the fluidized bed, the temperature decreases rapidly and the alkali molecules that escape from the fluidized bed nucleate to form new alkali aerosol particles, which are efficiently transported to the SID instruments with limited losses to the sampling lines [54,67].

3.1. Alkali concentrations during repeated redox cycles

Experiments were carried out using fluidized beds containing the three different OCs. Each experiment encompassed a series of successive redox cycles, during which the six distinct alkali salts were continuously introduced individually. The standard experimental protocol involved 2 to 4 redox cycles with KCl injection, succeeded by 2 to 4 cycles with KOH injection, and lastly followed by 2 to 4 cycles with K_2SO_4 injection. The same procedure was then followed for the sodium salts: NaCl, NaOH and

Table 1
Time durations in each gas condition for the different OC materials.

OC material	Period	Duration (s)
Calcium manganite ($CaMnO_3$)	Reducing	800
	Inert	180
	Oxidizing	1400
	Inert	180
Manganese oxide (Mn_3O_4)	Reducing	400
	Inert	180
	Oxidizing	800
	Inert	180
Ilmenite ($FeTiO_3$)	Reducing	550
	Inert	180
	Oxidizing	1600
	Inert	180

Na_2SO_4.

Fig. 2a illustrates experimental results obtained with a fluidized bed of 40 g Mn_3O_4 in the reactor. The colored fields indicate recurring inert (white), reducing (orange), and oxidizing (blue) conditions and each redox cycle is marked in red for clarity. The experiments started with continuous injection of KCl over several consecutive redox cycles, then proceeded with KOH, and finally K_2SO_4.

The results obtained with KCl demonstrate significant fluctuations in gas and alkali concentrations within each redox cycle, exhibiting high consistency across cycles. When the alkali inlet is switched from KCl to KOH, the alkali concentration is rapidly reduced to a low level indicating efficient uptake of the introduced KOH by the Mn_3O_4 particles and remains bound to the bed material regardless of the gas composition during the redox cycles. Subsequently, when KOH is replaced by K_2SO_4, the alkali signal reemerges, indicating less efficient uptake compared to KOH. The observed alkali concentrations are similar for KCl and K_2SO_4, suggesting a comparable degree of alkali uptake by Mn_3O_4. However, the specific pattern observed during a redox cycle differs for the two salts, underscoring the intricate nature of alkali-OC interactions, influenced by both the alkali salt type and the gas composition.

The results presented in Fig. 2b depict the outcomes of experiments involving sodium-containing compounds interacting with a fluidized bed of Mn_3O_4 particles. Qualitatively, these results mirror those obtained with potassium salts (Fig. 2a), showcasing an exceptionally efficient uptake of NaOH and similar patterns depending on gas composition during the redox cycle for NaCl and Na_2SO_4. Notably, the observed alkali concentration is considerably higher for NaCl in comparison to KCl, indicating a significant difference in their uptake efficiency, with NaCl exhibiting a greater likelihood of escaping from the fluidized bed.

Fig. 2c and d illustrate the results when the alkali salts interact with a fluidized bed comprising $CaMnO_3$. Parallel to the outcomes observed for

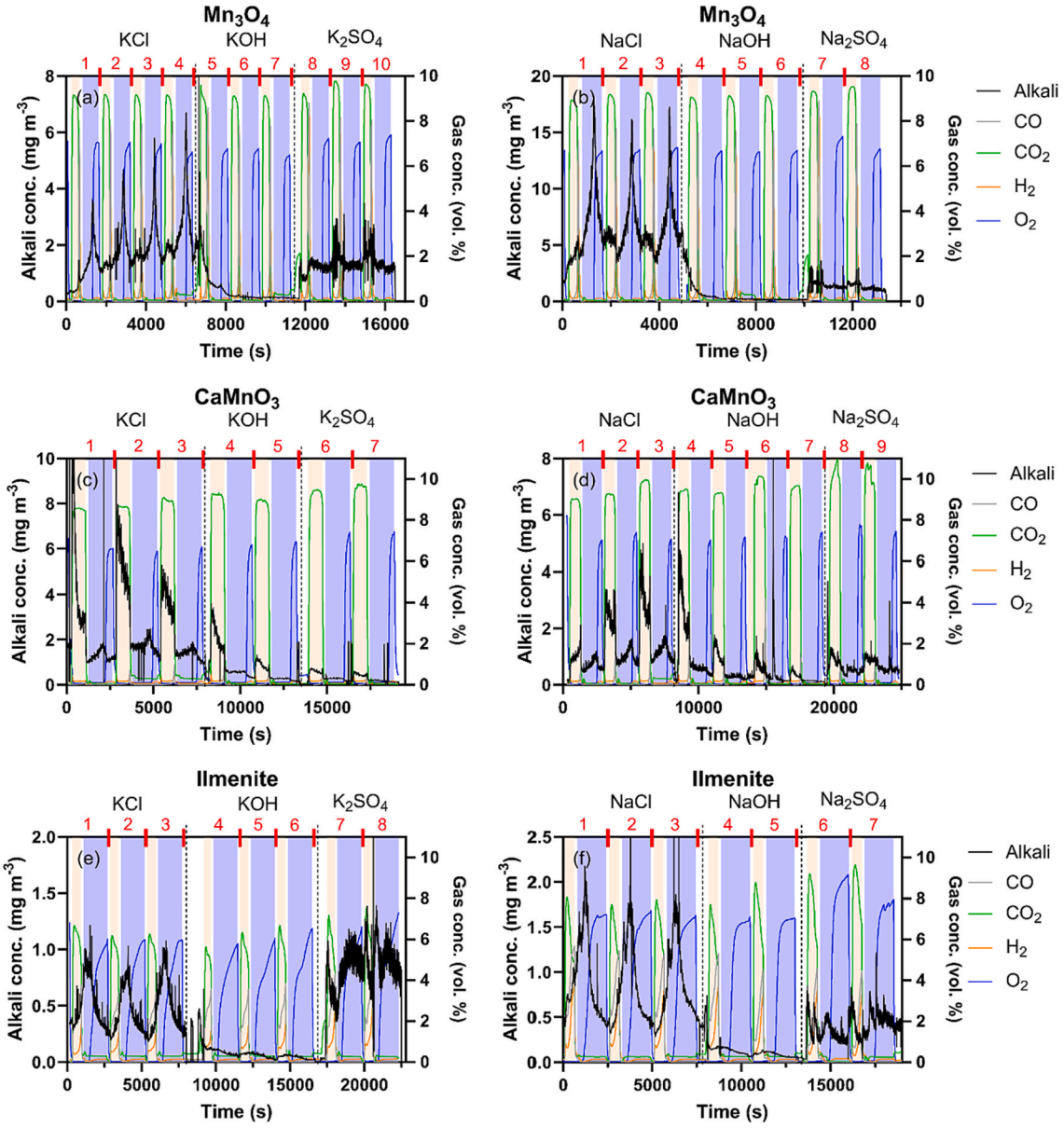

Fig. 2. Alkali (black line) and gas (colored lines, see legend) concentrations measured in the flux from the reactor during experiments with a fluidized bed consisting of 40 g of (a, b) Mn_3O_4, (c, d) $CaMnO_3$, and (e, f) ilmenite particles. Alkali-containing aerosol consisting of (a, c, e) KCl, KOH or K_2SO_4, and (b, d, f) NaCl, NaOH or Na_2SO_4 was continuously fed to the reactor during consecutive redox cycles (numbered and marked in red). The colored fields indicate recurring inert (white), reducing (orange) and oxidizing (blue) conditions. The reactor temperature was 900 °C. (For interpretation of the references to colour in this figure legend, the reader is referred to the web version of this article.)

Mn_3O_4, alkali chlorides tend to escape more readily from the fluidized bed in contrast to hydroxides and sulfates. However, the differences between the latter two are not as pronounced as observed for Mn_3O_4. Furthermore, alkali uptake is generally more efficient under oxidizing conditions compared to reducing conditions for all investigated alkali salts.

Adding 40 g of ilmenite OC particles to the reactor again results in a distinct behavior with respect to alkali-OC interactions (Fig. 2e and f). The outlet alkali concentration is notably lower for all alkali salts and under all conditions compared to the other fluidized bed materials. This aligns with the well-established capability of ilmenite to effectively capture alkali [6,51,53]. The different alkali compounds exhibit similar trends in the ilmenite experiments. Specifically, NaOH injection results in exceptionally low outlet alkali concentrations compared to NaCl and Na_2SO_4, which yield higher alkali concentrations.

The results displayed in Fig. 2 underscore the sensitivity of alkali uptake to the types of alkali salt, bed material, and gas composition. The findings are summarized in Fig. 3 showcasing the average alkali concentrations in reducing and oxidizing conditions for all alkali salt-OC combinations. The averages were calculated based on the final redox cycle run with each alkali compound. These findings highlight significant differences in alkali uptake efficiency among the fluidized bed materials, with ilmenite exhibiting the highest efficiency, followed by $CaMnO_3$ and Mn_3O_4.

Overall, alkali chlorides generally exhibit a higher tendency to escape from the bed materials compared to hydroxides and sulfates. Notably, an outstandingly efficient uptake of alkali hydroxides is observed on Mn_3O_4 and ilmenite compared to chlorides and sulfates. Furthermore, average alkali concentrations tend to be lower in oxidizing conditions than in reducing conditions for experiments involving $CaMnO_3$. In contrast, experiments with ilmenite and Mn_3O_4 often result in higher alkali concentrations in oxidizing conditions compared to reducing conditions.

3.2. Influence of the detailed redox process on alkali uptake

Single redox cycles are investigated in greater detail to characterize the influence of OC reduction and oxidation processes on the observed alkali uptake. Figs. 4–6present alkali concentrations as a function of time during these cycles in experiments involving the three OCs, while continuously introducing KCl, NaCl, KOH, NaOH, K_2SO_4, or Na_2SO_4 into the fluidized bed reactor.

Fig. 4 provides insights into experiments with 40 g of Mn_3O_4 within the reactor. The gas concentrations at the outlet indicate an effective reduction and oxidation of the OC material. The reducing stage shows high CO_2 and low CO and H_2 concentrations, indicating excellent gas conversion efficiency. Following approximately 350 s in the reducing stage, the OC is fully reduced and the CO_2 concentration drops while the CO and H_2 concentrations increase. The gas composition is shifted to inert gas soon after the reduction is completed, which is followed by the oxidation stage. The time duration required to fully oxidize the OC is approximately 500 s, after which the outlet O_2 concentration rapidly reaches the inlet concentration.

Fig. 4a and b show the alkali concentrations when KCl and NaCl are injected into the Mn_3O_4 fluidized bed. In both cases, the alkali concentration remains relatively constant throughout the reduction stage, and similar concentrations are observed during the adjacent inert stages. This suggests that alkali uptake is independent of the degree of reduction of the OC material. Interestingly, the alkali concentration increases as the OC oxidation process proceeds indicating less efficient alkali uptake

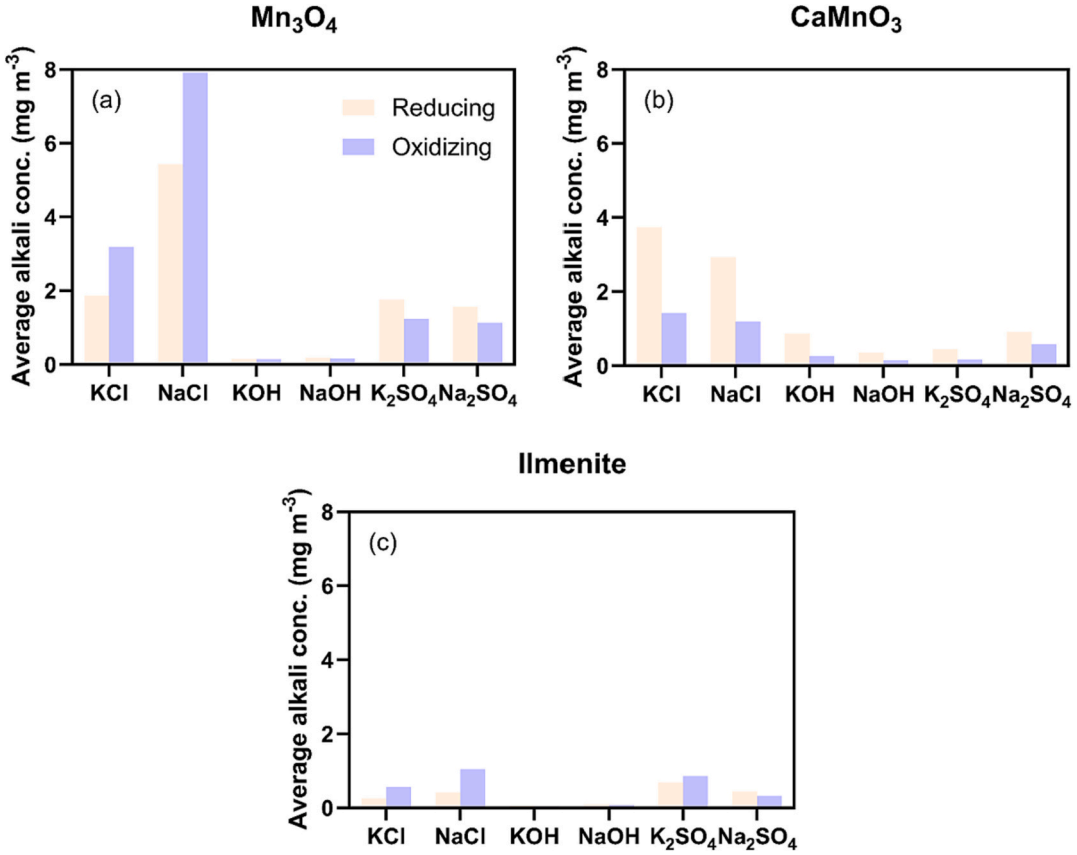

Fig. 3. Average alkali concentrations measured in the outlet gas flux from the reactor in reducing (orange) and oxidizing (blue) conditions when the fluidized bed consists of 40 g of (a) Mn_3O_4, (b) $CaMnO_3$ and (c) ilmenite particles. (For interpretation of the references to colour in this figure legend, the reader is referred to the web version of this article.)

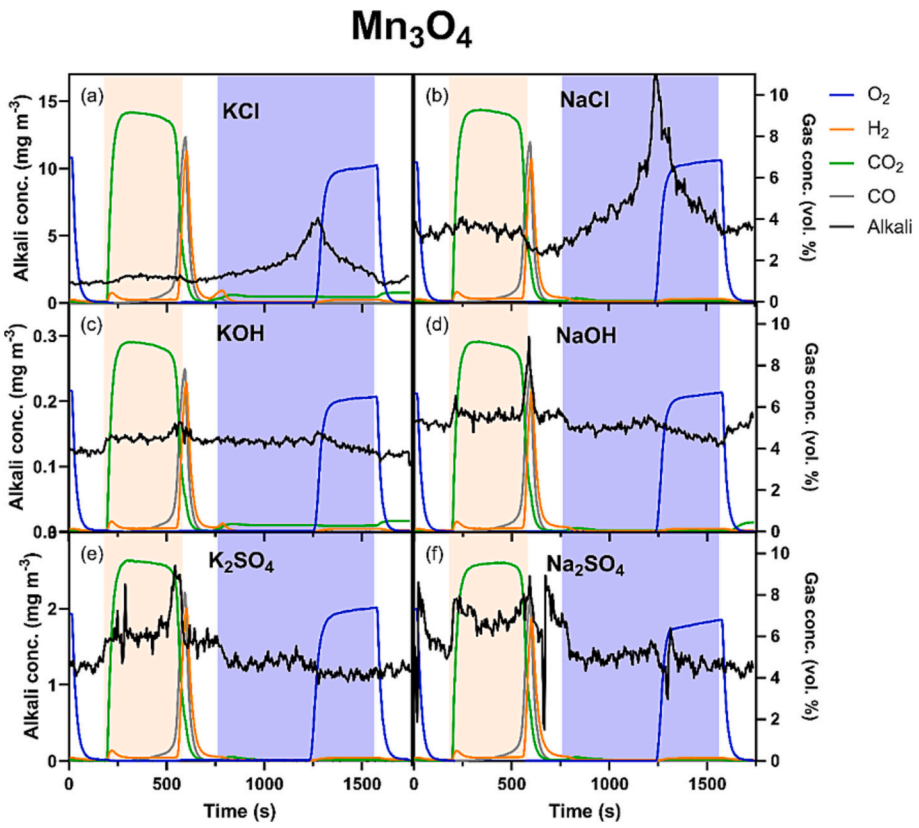

Fig. 4. Alkali (black lines) and gas concentrations (colored lines, see legend) measured during one redox cycle with 40 g fluidized bed of Mn_3O_4 and injection of (a) KCl, (b) NaCl, (c) KOH, (d) NaOH, (e) K_2SO_4 and (f) Na_2SO_4. Colored areas mark stages with oxidizing (blue), inert (white) and reducing (orange) atmospheres. (For interpretation of the references to colour in this figure legend, the reader is referred to the web version of this article.)

during this process. A notable peak in alkali concentration is observed around the time the OC becomes completely oxidized, with the concentration then gradually decreasing during the remaining approximately 250 s of the oxidation stage. The gradual adjustment to new steady state conditions suggests that the underlying process is characterized by kinetics on the time scale of the experiment.

The corresponding results for alkali hydroxides and sulfates interacting with Mn_3O_4 are displayed in Fig. 4c–f. As described earlier, the relative alkali levels are lower and comparable for the two alkali sulfates and markedly lower for the hydroxides compared to the alkali chlorides. In both cases, the observed concentrations remain relatively constant irrespective of gas composition. An exception is a minor peak in alkali concentration as the reduction stage nears completion.

The experiments conducted with the $CaMnO_3$ bed material are illustrated in Fig. 5. Similar to Mn_3O_4, the outlet gas concentrations show complete conversion of the fuel gases to CO_2 during the reducing period and complete O_2 uptake during the OC oxidation process. However, the time required to fully reduce and oxidize the $CaMnO_3$ is considerably longer compared to Mn_3O_4, since the former contains 40% active phase while the remaining 60% act as inert support material [47].

The experiments with $CaMnO_3$ yield notably different alkali concentration behaviors, in comparison to the Mn_3O_4 material. Higher concentrations are consistently observed during reducing conditions compared to inert or oxidizing conditions. In the reducing stage, a gradual decline in alkali concentration is noted for chlorides and hydroxides, implying an increasing alkali uptake as the oxygen fugacity within the OC material decreases. Conversely, the oxidizing period is characterized by lower and relatively stable alkali concentrations. Notably, a gradual increase in alkali concentration occurs around the time when the OC is fully oxidized for the chlorides, akin to the behavior observed for Mn_3O_4.

When the reactor is instead loaded with 40 g of ilmenite, notable differences in both gas and alkali concentrations are observed compared to the results obtained with the other bed materials (Fig. 6). The gas concentrations provide evidence of incomplete fuel conversion, with approximately 77% of CO being converted to CO_2 at the outset of the reducing stage. Simultaneously, merely 7% of the incoming H_2 is detected in the exhaust, signifying a more efficient conversion process. During the oxidizing stage, complete O_2 uptake is observed in the initial 300 s, followed by a gradual increase in O_2 concentration in the exhaust until the OC reaches full oxidation after approximately 1400 s. The alkali profiles exhibit overall low concentrations compared to Mn_3O_4 and $CaMnO_3$ and distinct differences in qualitative behavior for chlorides, hydroxides, and sulfates during both the reducing and oxidizing stages. Worth highlighting is that the peak around the 600 s time mark for the Na_2SO_4 experiment is a consequence of flow disturbances in the exhaust lines and should therefore not be considered when discussing overall trends.

In summary, the investigated systems exhibit a diverse array of behaviors during different stages of the redox cycle, depending on the specific properties of each system. Despite the diversity, a few general trends can be identified in the data. Potassium and sodium salts of the same type consistently demonstrate qualitatively similar patterns during the redox cycle, indicating substantial similarities in their interactions with various types of OCs. Notably, a qualitatively similar behavior is observed for alkali chlorides during the oxidizing stage. This behavior is consistently observed across all investigated OCs and suggest a distinctive role of chlorine in the observed results, warranting further study.

3.3. *Speciation of released alkali compounds*

To further characterize the outcome of the alkali-OC interactions, the

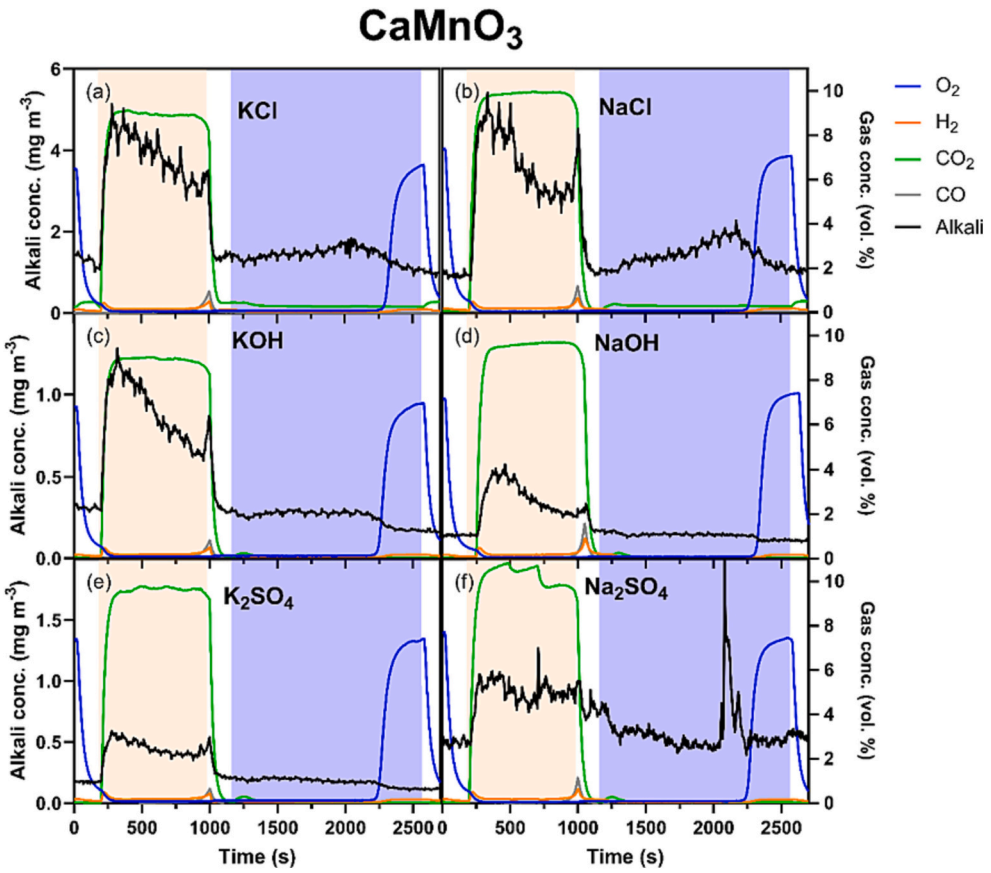

Fig. 5. Alkali (black lines) and gas concentrations (colored lines, see legend) measured during one redox cycle with 40 g fluidized bed of $CaMnO_3$ and injection of (a) KCl, (b) NaCl, (c) KOH, (d) NaOH, (e) K_2SO_4 and (f) Na_2SO_4. Colored areas mark stages with oxidizing (blue), inert (white) and reducing (orange) atmospheres. (For interpretation of the references to colour in this figure legend, the reader is referred to the web version of this article.)

various types of alkali species present in the outflow were characterized. The alkali concentration results presented above were obtained with a SID operated with a constant platinum filament temperature of 1100 °C (referred to as SID1 in Fig. 1). In parallel, a second SID (SID2) was operated with a filament temperature that alternated between three temperatures according to the following repeated sequence: 550–1100–800–1100 °C. The alkali signals obtained at the three different temperatures together with the transient signals produced by repeatedly raising the filament temperature to 1100 °C depend on the molecular composition of the alkali species. This behavior was utilized to determine the contributions of alkali chlorides, hydroxides, carbonates and sulfates to the flux from the reactor.

Details regarding the innovative speciation method are presented in Appendix A. Included in the alkali species analysis are compounds of K^+ and Na^+ bound to Cl^-, OH^-, CO_3^{2-} and SO_4^{2-}. The relative contribution of different alkali species is reported for each investigated alkali salt-OC combination. The analysis distinguishes between reducing and oxidizing conditions and the used experimental values are average values obtained under stable reducing or oxidizing conditions.

Fig. 7 summarizes the results from the speciation analysis where the relative contribution of each alkali compound is displayed for all investigated cases. In the case of KCl injection to the three types of OC beds, KCl is also the dominating alkali species in the outflow from the reactor under both oxidizing and reducing conditions. This is according to expectations since the inlet KCl concentration is relatively high. Alkali chlorides are also known to be highly volatile and KCl is often observed during solid fuel conversion if chlorine is present in sufficient concentrations [16,68,69]. The observation of minor contributions from other alkali compounds is likely due to limitations in the speciation methodology rather than actual formation of these compounds.

The results for NaCl are similar to the KCl injection results. NaCl is the dominating species in the outflow and minor contributions from other compounds cannot be conclusively shown to be present. The only exception is the case of ilmenite under reducing conditions where Na_2SO_4 appears to dominate rather than NaCl. This may be due to limitations in the speciation methodology where two mixtures of alkali salts under unfavorable conditions give similar results in the analysis.

We next focus on the cases where K_2SO_4 and Na_2SO_4 are injected to the fluidized. In both cases, the respective sulfate emerges as the predominant alkali compound in the reactor's outflow, and the present analysis does not conclusively confirm substantial contributions from other compounds.

The distinct patterns observed for chlorides and sulfates do not replicate for alkali hydroxides. The outflow appears to comprise a more complex mixture of alkali salts compared to the other cases. Alkali hydroxides make minor contributions in several experiments, e.g., in the case of $CaMnO_3$ under reducing conditions and ilmenite in oxidizing conditions, but significant variability of the hydroxide conditions is observed depending on the investigated system. The low alkali concentrations observed in alkali hydroxide injection experiments (Fig. 3), influence the accuracy of the analysis. On the other hand, hydroxides exhibit a distinct dependence on SID filament temperature, aiding their differentiation from other alkali compounds in the speciation analysis. In conclusion, it is unlikely that alkali hydroxides would escape from the OC fluidized beds under investigation. This results in low concentrations of alkali hydroxides in the exhausts, and the availability of other counter-ions like Cl^- or SO_4^{2-} may significantly contribute to alkali release.

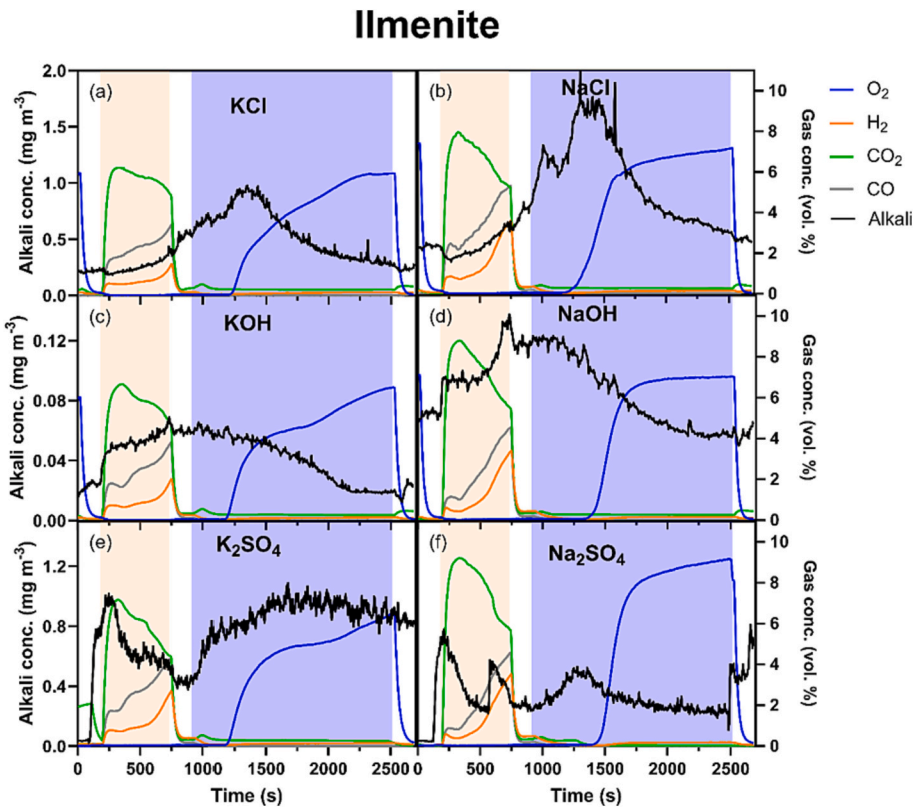

Fig. 6. Alkali (black lines) and gas concentrations (colored lines, see legend) measured during one redox cycle with 40 g fluidized bed of ilmenite and injection of (a) KCl, (b) NaCl, (c) KOH, (d) NaOH, (e) K_2SO_4 and (f) Na_2SO_4. Colored areas mark stages with oxidizing (blue), inert (white) and reducing (orange) atmospheres. (For interpretation of the references to colour in this figure legend, the reader is referred to the web version of this article.)

4. Discussion

4.1. Methodological considerations

The current study relies on a recent advancement in reactor design [54,56], and is the first extensive investigation utilizing this novel reactor. Specifically engineered inlet and outlet systems aim to reduce alkali-wall interactions to a minimum [56]. The temperature is efficiently quenched after the fluidized bed causing alkali compounds to form aerosol particles that are efficiently transported to the online alkali measurement devices. The present study confirms the functionality of the experimental setup under diverse conditions and with varying materials. A remaining concern requiring further exploration pertains to characterizing any potential remaining minor losses of alkali to reactor walls [56]. Consequently, absolute uptake efficiencies are not the primary focus here, and instead relative uptake efficiencies are reported, enabling comparisons across multiple systems. An ideal benchmark case for comparison would involve a bed material that does not absorb alkali under the elevated temperature conditions of interest, although such a system is yet to be identified and characterized.

A second critical innovation employed in this study is the utilization of the SID, particularly the step-wise filament temperature modulation technique for alkali speciation, a technique used for the first time in this study. The SID instrument, known for its sensitivity and selectivity towards alkali, had previously been utilized solely for determining total alkali concentrations, lacking the ability to distinguish between K, Na, and different counter-ions. This study demonstrates the potential of the temperature modulation technique for online speciation of alkali compounds, marking it as a valuable tool for thermal conversion studies and related research. Ongoing development efforts should focus on optimizing the temperature modulation technique concerning selectivity and time resolution.

The study was conducted following an experimental protocol where the type of injected alkali salt was regularly changed. Consequently, there exists a risk of memory effects where salt adsorbed earlier during the experiment may influence results obtained during subsequent salt injections. The experimental results in Fig. 2 indicate that the observed alkali pattern swiftly changes when transitioning to a new type of alkali salt, and this new pattern seems to be consistent in subsequent redox cycles. Transient behavior indicating memory effects is most evident when transitioning from chlorides to hydroxides. In this case, the effects could be accentuated by the substantial difference in uptake efficiency between chlorides and hydroxides, potentially influenced by remaining chlorine promoting alkali escape from the fluidized bed. Based on the available experimental data, it is concluded that some memory effects can be identified, but the effects are minor after two or more redox cycles and have a limited impact on reported results.

4.2. Alkali interactions with oxygen carrier materials

The fluidized bed provides a large surface area for alkali-OC interactions, and it is likely that all injected alkali molecules interact efficiently with the bed material. This is supported by the close to 100% alkali hydroxide uptake in some cases. Molecules that reach the OC surface will initially adsorb and may thereafter either desorb or continue to interact with the surface layer. The adsorbed molecules may undergo a range of subsequent processes, including dissociation, diffusion in the surface layer, diffusion into the bulk, and association with new counter-ions followed by desorption. The experimental results suggest that one major outcome is that alkali forms strong bonds to the surface or within the bulk of the material, where they largely remain on the time-scale of the experiments.

The alkali uptake depends on the properties of the injected alkali compounds and the OC materials. A qualitatively similar behavior is

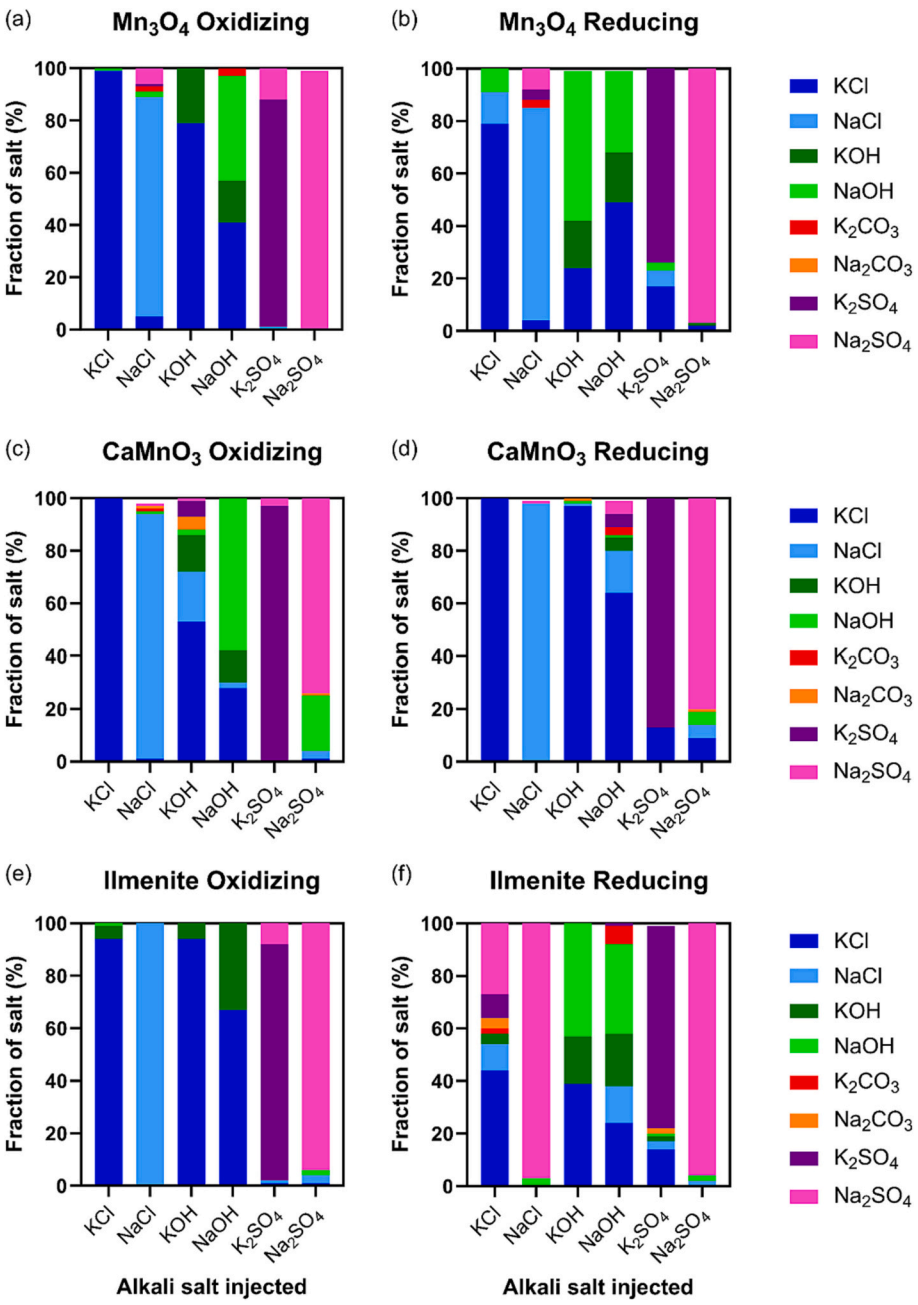

Fig. 7. Percentage of each alkali salt leaving the reactor during experiments using fluidized beds of (a, b) Mn_3O_4, (c, d) $CaMnO_3$ and (e, f) ilmenite with continuous injection of aerosols: KCl, NaCl, KOH, NaOH, K_2SO_4 or Na_2SO_4. Measurements under (a, c, e) oxidizing conditions and (b, d, f) reducing conditions utilized a SID with a filament temperature alternating between 550, 800 and 1100 °C; see text and Appendix A for details about the SID methodology.

observed when sodium and potassium salts of the same type are introduced to the reactor. Sodium compounds are in general more stable and less reactive than potassium compounds [20,70], [71]. However, the temperature is relatively high in this study, which should act to reduce the differences in behavior between the two types of compounds.

In contrast, the counter-ions (Cl^-, OH^- and SO_4^{2-}) have a considerably larger influence on the results. The highest alkali concentrations are observed during alkali chloride injection, followed by alkali sulfate injection. Chlorides and sulfates are also the dominating compounds in the outflow when these salts are injected, confirming that a fraction of the salts can survive transport through the utilized fluidized beds. It is likely that the availability of chlorine and sulfur compounds in the OC surface layers enhances the probability of recombination to form volatile compounds that may eventually escape from the fluidized bed.

The behavior of alkali hydroxides is more intriguing. The hydroxides are to large extent lost to the OCs (Fig. 3). The alkali that escape from the beds during alkali hydroxide injection is often dominated by other counter-ions including chlorine (Fig. 7). The results suggest that adsorbed alkali hydroxides are less likely to escape from the bed materials, indicating that they are less likely to recombine and desorb from the OC materials. Similar observations have been reported in a previous study, where thermodynamic calculations show that KOH(g) is present during combustion of fuels with particularly low Cl and S content [52]. Combustion of fuels where Cl or S is present in sufficient amounts shows predominant alkali release in the form of alkali chlorides and alkali sulphates [52]. However, Dayton et al. have shown that alkali hydroxide formation increases when steam is added to the combustion environment [72], which may explain the higher alkali outlet concentrations

during the reduction of $CaMnO_3$ (Fig. 5c).

The alkali uptake is influenced by the detailed chemical properties of the bed materials under reducing and oxidizing conditions, and the relevant chemical transformations for the three bed materials are therefore briefly reviewed and related to the experimental observations. Mn_3O_4 is the most likely form of manganese under oxidizing CLC conditions, which is transformed into MnO in reducing atmosphere [46]. Further reduction from MnO to Mn is not possible at atmospheric pressure [9], and the two most oxidized forms of manganese (MnO_2 and Mn_2O_3) decompose in air at temperatures around 516 and 820 °C and are not expected to be present in CLC [46]. The Mn_3O_4-MnO system has approximately twice as much free oxygen available compared to the Fe_2O_3-Fe_3O_4 system [47]. The bed material used in this study, however, consists to 60 mass% of inert Mg-ZrO_2, resulting in an active amount of free oxygen around 3 mass% [47]. In addition, the reactivity of manganese oxide is determined by its degree of crystallization. These observations relates to the sintering temperature of which the OC particles are prepared. While sintering should be done at a high temperature to improve the mechanical integrity of the particles, this leads to reduced reactivity due to a higher degree of crystallization [47]. The present experimental results show a weak alkali uptake dependence on gas composition for Mn_3O_4 (Fig. 4), suggesting that the transition between Mn_3O_4 and MnO does not have a major impact on alkali bound to the bed material. The exception is the remarkable behavior of alkali chlorides during the OC oxidation process, with a peak in alkali emission around the time when the oxidation process is completed (Fig. 4). Similar behavior is observed for the other two OCs and does consequently not appear to be directly related to the detailed surface structure. To our knowledge no earlier studies of the alkali-Mn_3O_4 system have been carried out that can contribute to the present understanding of the system.

The $CaMnO_3$ bed material displays a more complex chemistry during a redox cycle. Materials of perovskite structure, such as the $CaMn_{0.775}Ti_{0.125}Mg_{0.1}O_{3-\delta}$ used here, have a unit cell with the general formula $ABO_{3-\delta}$, where A (Ca in this case) is a large cation and B (Mn or Ti in this case) is a smaller cation. The degree of oxygen deficiency is described by the δ-factor, and equals zero for a perfect structure [73]. Since the δ-factor can be altered by changing the thermodynamic properties of the surroundings, these materials are interesting for CLC. The oxidizing and reducing conditions in the AR and FR, respectively, result in a smaller δ_{AR} compared to δ_{FR} where the difference between them determine how much oxygen will be available for oxidation according to reaction (1) [74]:

$$ABO_{3-\delta_{AR}} \leftrightarrow ABO_{3-\delta_{FR}} + 1/2(\delta_{FR} - \delta_{AR})O_2 \quad (1)$$

In addition, the amount of O_2 that can be transferred from high-to-low O_2 atmospheres depends on the O_2 partial pressure used for oxidation [74]. The mechanism was demonstrated where $CaMn_{0.875}Ti_{0.125}O_{3-\delta}$ released considerably more O_2 after being oxidized in air compared to a mixture of 5% O_2 in N_2 [34]. It is further believed that addition of Ti could increase the structural integrity of the perovskite at high temperatures, by preventing material decomposition into Ca_2MnO_4 and $CaMn_2O_4$, which could otherwise hinder the reoxidation processes [74]. The present experimental results for the $CaMnO_3$ system show that alkali uptake is considerably less efficient under reducing conditions compared to oxidizing conditions for all types of alkali salts. It thus appears that the stability of K and Na on the OC surface is directly affected by the oxygen deficiency under reducing conditions. Similar to the alkali-Mn_3O_4 system, we are not aware of an earlier study of the alkali-$CaMnO_3$ interactions discussed here.

In contrast, the ilmenite mineral has been studied in greater detail, including studies of alkali interactions with the material. The oxidation of ilmenite involves two key steps: (i) the conversion of Fe^{2+} to Fe^{3+} and (ii) the formation of phases enriched in both Fe and Ti [75]. The conversion of Fe^{2+} to Fe^{3+} is considered as the most crucial step in the oxidation process and occurs initially through surface ion diffusion, followed by slower lattice diffusion. Iron diffuses out of the ilmenite structure during the oxidation process, resulting in the formation of a surface hematite (Fe_2O_3) layer and needle-like rutile (TiO_2) texture within the sample [76]. The hematite layer grows during repeated oxidation and reduction cycles, which is typically referred to as ilmenite activation [77]. Gibbs free energies were calculated for reactions between alkali hydroxide and hematite using the reaction module in FactSage 8.2 [78]. The result was negative Gibbs free energies for both the reaction between KOH and hematite ($\Delta G_{900°C} = -60$ kJ) and NaOH with hematite ($\Delta G_{900°C} = -80$ kJ). While the thermodynamics suggest that both reactions are spontaneous, the lower ΔG favors the NaOH reaction over the corresponding potassium hydroxide reaction [78]. The alkali interactions with ilmenite has recently been investigated in a few experimental studies [5,6,51–53]. Potassium has been observed to diffuse into the particles, leading to the formation of compounds with titanium oxides, such as $KTi_8O_{16.5}$ [6] while concurrently an outward migration of iron is observed [51]. The segregation between iron and alkali elements is commonly achieved through a process known as alkali roasting, which is employed in industrial applications for the purification of TiO_2 from ilmenite. In this process, K_2CO_3 and NaOH are utilized to enhance the separation between iron and titanium [13]. Furthermore, absorption of potassium does not appear to induce agglomeration of the ilmenite bed material [6,51], a concern that arises when using sand or other silica-containing bed materials [14,15,79]. However, the impact of alkali absorption on the reactivity of the material or the availability of iron on the surface of the particles, which could affect oxygen transfer efficiency, remains uncertain.

The present study indicates that a rich alkali chemistry occurs on the studied bed materials, but does not provide information about the detailed alkali uptake mechanisms and state of alkali on the materials in various conditions. There is thus a need for studies with complementary surface sensitive techniques, including both ex situ methods and in situ techniques under conditions relevant to CLC.

4.3. Implications for chemical looping combustion of biomass

The findings of this study can be utilized to examine the characteristics of alkali in a CLC process comprising interconnected air and fuel reactors. Alkali is abundant in biofuels and is therefore introduced into the fuel reactor of a CLC system along with the fuel. As a consequence of the fuel conversion, a fraction of the alkali is released into the gas phase. According to the present study, the extent of gaseous alkali uptake varies between fluidized beds of calcium manganite, ilmenite and manganese oxide.

We begin by focusing on the results during reducing conditions, i.e., the implications for the fuel reactor in a CLC system. The results in this study show near complete uptake of the injected alkali by ilmenite during experiments with KCl, NaCl, KOH or NaOH in reducing conditions. In practice, this would result in low alkali emissions in the flue gases leaving the fuel reactor. The extensive alkali uptake is in accordance with previous findings, showing that ilmenite is an effective alkali scavenger [6,51]. However, the time the OC material spends in the present reactor is very short compared to the lifetime of the bed in a commercial conversion application [80], and the alkali bound to the ilmenite may approach saturation during long periods of operation. Compared to ilmenite, calcium manganite or manganese oxide allows a more significant fraction of the injected alkali to escape from the reactor.

Most of the heat extraction equipment in a CLC unit is placed in the gas stream leaving the exothermic air reactor, and it is therefore of importance to limit the emissions of corrosive alkali compounds from this reactor [2]. Although alkali is fed to the system with the fuel, i.e., to the reducing fuel reactor side, fractions of the alkali can be transferred over to the air reactor, either as solid ash particles, or on the surface of OC particles [5]. The low alkali concentrations in oxidizing conditions during ilmenite and calcium manganite operation is, therefore, beneficial with regard to CLC operation. In comparison, the alkali outlet

concentrations are significantly higher during operation with manganese oxide, thus showing less efficient alkali uptake. It should be noted that the current experiments are carried out with continuous alkali injection, which may affect the comparison with a real CLC system where the main alkali emissions from the fuel occur under reducing conditions in the fuel reactor.

Overall, the results show that ilmenite outperform the calcium manganite and manganese oxide with respect to reducing the gaseous alkali concentrations. On the other hand, the calcium manganite and manganese oxide materials perform significantly better with regard to fuel conversion and oxidizing efficiency. The accumulation of alkali by the ilmenite may also improve the fuel conversion due to the catalytic properties of alkali [81], which has not been considered in this study.

5. Conclusions

Experiments have been carried out to evaluate the interactions between different alkali salt compounds with three different OC materials used in CLC of biomass. Alkali in the form of KCl, NaCl, KOH, NaOH, K_2SO_4 and Na_2SO_4 aerosol particles were fed to a 40 g fluidized bed of calcium manganite, ilmenite or manganese oxide at 900 °C temperature. The experiments were conducted under recurring reducing, inert and oxidizing conditions to simulate the different environments of a CLC system. The key findings can be summarized as follows:

- The experiments demonstrate that the presence of a fluidized bed of OC particles significantly influence the outlet alkali concentrations, indicating efficient uptake of alkali by the OC materials.
- The type of OC material plays a crucial role in alkali uptake, with calcium manganite, manganese oxide, and ilmenite exhibiting varying levels of efficiency depending on the gas conditions. Among them, ilmenite showed near-complete uptake of alkali, especially during reducing conditions, making it a promising option for reducing alkali emissions.
- The alkali speciation analysis revealed that NaCl and KCl were the predominant alkali species emitted during NaCl and KCl injection. Likewise, alkali sulfates were the dominating species during alkali sulfate injection, while alkali hydroxide injection resulted in low emissions dominated by alkali hydroxides and chlorides.
- Furthermore, the study highlights the importance of trade-off between alkali uptake efficiency and fuel conversion/oxidizing efficiency of the OC materials, and while ilmenite demonstrated excellent alkali uptake, manganese oxide and calcium manganite exhibited superior fuel conversion and oxidizing efficiency.

Overall, the experimental results demonstrate the complex behavior of alkali in the CLC process, influenced by factors such as gas conditions, OC bed material, and alkali salt compounds. In conclusion, ilmenite stands out as a promising OC material for reducing gaseous alkali emissions in CLC systems, particularly due to its high alkali uptake and preference for less corrosive alkali sulphates. However, considerations must be given to long-term operation and potential alkali saturation. Calcium manganite and manganese oxide also exhibited advantages in terms of fuel conversion and oxidizing efficiency. Achieving low concentrations of gaseous alkali emissions, especially on the air reactor side, remains crucial for maintaining the integrity of heat exchanger surfaces.

The findings of this study contribute to a deeper understanding of alkali behavior in biomass thermal conversion systems and provide valuable insights for the design and optimization of CLC processes. Future research should explore the influence of alkali concentration and temperature on the investigated processes, the long-term performance of OC materials including studies of aged OCs, and the catalytic effects of alkali on fuel conversion.

CRediT authorship contribution statement

Viktor Andersson: Formal analysis, Investigation, Methodology, Writing – original draft, Writing – review & editing. **Xiangrui Kong:** Supervision, Writing – review & editing. **Henrik Leion:** Resources. **Tobias Mattisson:** Supervision, Writing – review & editing. **Jan B.C. Pettersson:** Conceptualization, Formal analysis, Resources, Supervision, Writing – review & editing.

Declaration of competing interest

The authors declare that they have no known competing financial interests or personal relationships that could have appeared to influence the work reported in this paper.

Data availability

Data will be made available on request.

Acknowledgments

This work is supported by the Swedish Research Council, project “Biomass combustion chemistry with oxygen carriers” 2016-06023.

Appendix A. Supplementary data

Supplementary data to this article can be found online at https://doi.org/10.1016/j.fuproc.2023.108029.

References

[1] J. Adánez, A. Abad, T. Mendiara, P. Gayán, L.F. de Diego, F. García-Labiano, Chemical looping combustion of solid fuels, Prog. Energy Combust. Sci. 65 (2018) 6–66, https://doi.org/10.1016/j.pecs.2017.07.005.
[2] A. Lyngfelt, Chemical looping combustion: status and development challenges, Energy Fuel 34 (8) (2020) 9077–9093, https://doi.org/10.1021/acs.energyfuels.0c01454.
[3] A. Lyngfelt, B. Leckner, T. Mattisson, A fluidized-bed combustion process with inherent CO2 separation; application of chemical-looping combustion, Chem. Eng. Sci. 56 (10) (2001) 3101–3113, https://doi.org/10.1016/S0009-2509(01)00007-0.
[4] A. Lyngfelt, Oxygen carriers for chemical looping combustion – 4 000 h of operational experience, Oil Gas Sci. Technol. Rev. IFP Energ. nouvell. 66 (2) (2011) 161–172, https://doi.org/10.2516/ogst/2010038.
[5] I. Gogolev, C. Linderholm, D. Gall, M. Schmitz, T. Mattisson, et al., Chemical-looping combustion in a 100 kW unit using a mixture of synthetic and natural oxygen carriers – operational results and fate of biomass fuel alkali, In. J. Greenh. Gas Control 88 (2019) 371–382, https://doi.org/10.1016/j.ijggc.2019.06.020.
[6] A. Corcoran, P. Knutsson, F. Lind, H. Thunman, Mechanism for migration and layer growth of biomass ash on ilmenite used for oxygen carrier aided combustion, Energy Fuel 32 (8) (2018) 8845–8856, https://doi.org/10.1021/acs.energyfuels.8b01888.
[7] R. Faust, T. Berdugo Vilches, P. Malmberg, M. Seemann, P. Knutsson, Comparison of ash layer formation mechanisms on Si-containing bed material during dual fluidized bed gasification of woody biomass, Energy Fuel 34 (7) (2020) 8340–8352, https://doi.org/10.1021/acs.energyfuels.0c00509.
[8] F. Störner, F. Hildor, H. Leion, M. Zevenhoven, L. Hupa, M. Rydén, Potassium ash interactions with oxygen carriers steel converter slag and iron mill scale in chemical-looping combustion of biomass—experimental evaluation using model compounds, Energy Fuel 34 (2) (2020) 2304–2314, https://doi.org/10.1021/acs.energyfuels.9b03616.
[9] A. Khanna, High Temperature Oxidation and Corrosion, 2002, https://doi.org/10.1142/9789814675239_0001.
[10] E. Hupa, E. Vainio, P. Yrjas, M. Engblom, M. Hupa, Corrosion of superheater materials by alkali chloride salt mixtures-the role of the presence of molten phase, FUEL 344 (2023), https://doi.org/10.1016/j.fuel.2023.128063.
[11] T. Jonsson, H. Larsson, S. Karlsson, H. Hooshyar, M. Sattari, et al., High-temperature oxidation of FeCr(Ni) alloys: the behaviour after breakaway, Oxid. Met. 87 (3) (2017) 333–341, https://doi.org/10.1007/s11085-017-9731-7.
[12] J. Lehmusto, P. Yrjas, Reactions of Potassium Chloride with Chromium as a First Step Towards High Temperature Corrosion in Biomass Combustion, 2019.
[13] F. Hildor, M. Zevenhoven, A. Brink, L. Hupa, H. Leion, Understanding the interaction of potassium salts with an ilmenite oxygen carrier under dry and wet conditions, ACS Omega 5 (36) (2020) 22966–22977, https://doi.org/10.1021/acsomega.0c02538.
[14] I. Staničić, V. Andersson, M. Hanning, T. Mattisson, R. Backman, H. Leion, Combined manganese oxides as oxygen carriers for biomass combustion — ash

interactions, Chem. Eng. Res. Des. 149 (2019) 104–120, https://doi.org/10.1016/j.cherd.2019.07.004.
[15] M. Öhman, A. Nordin, B.-J. Skrifvars, R. Backman, M. Hupa, Bed agglomeration characteristics during fluidized bed combustion of biomass fuels, Energy Fuel 14 (1) (2000) 169–178, https://doi.org/10.1021/ef990107b.
[16] A.A. Khan, W. de Jong, P.J. Jansens, H. Spliethoff, Biomass combustion in fluidized bed boilers: potential problems and remedies, Fuel Process. Technol. 90 (1) (2009) 21–50, https://doi.org/10.1016/j.fuproc.2008.07.012.
[17] Z.-M. He, J.-P. Cao, X.-Y. Zhao, Review of biomass agglomeration for fluidized-bed gasification or combustion processes with a focus on the effect of alkali salts, Energy Fuel 36 (16) (2022) 8925–8947, https://doi.org/10.1021/acs.energyfuels.2c01183.
[18] L. Yang, W. Chen, C. Song, C. Li, J. Chen, et al., Improving attrition resistance of oxygen carriers by biomass ash in chemical looping process, Fuel 346 (2023) 128352, https://doi.org/10.1016/j.fuel.2023.128352.
[19] Y.X. Ge, S.M. Ding, X.R. Kong, E. Kantarelis, K. Engvall, et al., Effects of used bed materials on char gasification: investigating the role of element migration using online alkali measurements, Fuel Process. Technol. 238 (2022), https://doi.org/10.1016/j.fuproc.2022.107491.
[20] J. Yu, Q. Guo, Y. Gong, L. Ding, J. Wang, G. Yu, A review of the effects of alkali and alkaline earth metal species on biomass gasification, Fuel Process. Technol. 214 (2021) 106723, https://doi.org/10.1016/j.fuproc.2021.106723.
[21] K. Mitsuoka, S. Hayashi, H. Amano, K. Kayahara, E. Sasaoaka, M.A. Uddin, Gasification of woody biomass char with CO2: the catalytic effects of K and Ca species on char gasification reactivity, Fuel Process. Technol. 92 (1) (2011) 26–31, https://doi.org/10.1016/j.fuproc.2010.08.015.
[22] J. Wei, X. Song, Q. Guo, L. Ding, K. Yoshikawa, G. Yu, Reactivity, synergy, and kinetics analysis of CO2 CO-pyrolysis/Co-gasification of biomass after hydrothermal treatment and coal blends, Energy Fuel 34 (1) (2020) 294–303, https://doi.org/10.1021/acs.energyfuels.9b03721.
[23] C. Dupont, T. Nocquet, J.A. Da Costa, C. Verne-Tournon, Kinetic modelling of steam gasification of various woody biomass chars: influence of inorganic elements, Bioresour. Technol. 102 (20) (2011) 9743–9748, https://doi.org/10.1016/j.biortech.2011.07.016.
[24] C. Dupont, S. Jacob, K.O. Marrakchy, C. Hognon, M. Grateau, et al., How inorganic elements of biomass influence char steam gasification kinetics, Energy 109 (2016) 430–435, https://doi.org/10.1016/j.energy.2016.04.094.
[25] O. Karlström, M.J. Dirbeba, M. Costa, A. Brink, M. Hupa, Influence of K/C ratio on gasification rate of biomass chars, Energy Fuel 32 (10) (2018) 10695–10700, https://doi.org/10.1021/acs.energyfuels.8b02288.
[26] Y.X. Ge, S.M. Ding, X.R. Kong, E. Kantarelis, K. Engvall, J.B.C. Pettersson, Real-time monitoring of alkali release during CO2 gasification of different types of biochar, Fuel 327 (2022), https://doi.org/10.1016/j.fuel.2022.125102.
[27] Y. Ge, S. Ding, W. Zhang, X. Kong, K. Engvall, J.B.C. Pettersson, Effect of fresh bed materials on alkali release and thermogravimetric behavior during straw gasification, Fuel 336 (2023) 127143, https://doi.org/10.1016/j.fuel.2022.127143.
[28] I. Staničić, T. Mattisson, R. Backman, Y. Cao, M. Rydén, Oxygen carrier aided combustion (OCAC) of two waste fuels - experimental and theoretical study of the interaction between ilmenite and zinc, copper and lead, Biomass Bioenergy 148 (2021) 106060, https://doi.org/10.1016/j.biombioe.2021.106060.
[29] M. Rydén, M. Hanning, A. Corcoran, F. Lind, Oxygen Carrier Aided Combustion (OCAC) of wood chips in a semi-commercial circulating fluidized bed boiler using manganese ore as bed material, Appl. Sci. 6 (11) (2016) 347, https://doi.org/10.3390/app6110347.
[30] O. Condori, F. García-Labiano, L.F. de Diego, M.T. Izquierdo, A. Abad, J. Adánez, Biomass chemical looping gasification for syngas production using ilmenite as oxygen carrier in a 1.5 kWth unit, Chem. Eng. J. 405 (2021) 126679, https://doi.org/10.1016/j.cej.2020.126679.
[31] F. Lind, N. Berguerand, M. Seemann, H. Thunman, Ilmenite and nickel as catalysts for upgrading of raw gas derived from biomass gasification, Energy Fuel 27 (2) (2013) 997–1007, https://doi.org/10.1021/ef302091w.
[32] T. Mattisson, M. Keller, C. Linderholm, P. Moldenhauer, M. Rydén, et al., Chemical-looping technologies using circulating fluidized bed systems: Status of development, Fuel Process. Technol. 172 (2018) 1–12, https://doi.org/10.1016/j.fuproc.2017.11.016.
[33] D. Karami, A.H. Soleimanisalim, M.H. Sedghkerdar, N. Mahinpey, Preparation of novel oxygen carriers supported by Ti, Zr-shelled γ-alumina for chemical looping combustion of methane, Ind. Eng. Chem. Res. 59 (7) (2020) 3221–3228, https://doi.org/10.1021/acs.iecr.9b06832.
[34] M. Rydén, A. Lyngfelt, T. Mattisson, CaMn0.875Ti0.125O3 as oxygen carrier for chemical-looping combustion with oxygen uncoupling (CLOU)—experiments in a continuously operating fluidized-bed reactor system, In. J. Greenh. Gas Control 5 (2) (2011) 356–366, https://doi.org/10.1016/j.ijggc.2010.08.004.
[35] C. Linderholm, M. Schmitz, P. Knutsson, A. Lyngfelt, Chemical-looping combustion in a 100-kW unit using a mixture of ilmenite and manganese ore as oxygen carrier, Fuel 166 (2016) 533–542, https://doi.org/10.1016/j.fuel.2015.11.015.
[36] M. Schmitz, C.J. Linderholm, Performance of calcium manganate as oxygen carrier in chemical looping combustion of biochar in a 10kW pilot, Appl. Energy 169 (2016) 729–737, https://doi.org/10.1016/j.apenergy.2016.02.088.
[37] J. Adanez, A. Abad, F. Garcia-Labiano, P. Gayan, L.F. de Diego, Progress in chemical-looping combustion and reforming technologies, Prog. Energy Combust. Sci. 38 (2) (2012) 215–282, https://doi.org/10.1016/j.pecs.2011.09.001.
[38] M. Källén, M. Rydén, C. Dueso, T. Mattisson, A. Lyngfelt, CaMn0.9Mg0.1O3-δ as oxygen carrier in a gas-fired 10 kWthChemical-looping combustion unit, Ind. Eng. Chem. Res. 52 (21) (2013) 6923–6932, https://doi.org/10.1021/ie303070h.
[39] D. Jing, M. Jacobs, P. Hallberg, A. Lyngfelt, T. Mattisson, Development of CaMn0.775Mg0.1Ti0.125O3-δ oxygen carriers produced from different Mn and Ti sources, Mater. Des. 89 (2016) 527–542, https://doi.org/10.1016/j.matdes.2015.09.117.
[40] H. Leion, Y. Larring, E. Bakken, R. Bredesen, T. Mattisson, A. Lyngfelt, Use of CaMn0.875Ti0.125O3 as oxygen carrier in chemical-looping with oxygen uncoupling, Energy Fuel 23 (10) (2009) 5276–5283, https://doi.org/10.1021/ef900444d.
[41] H. Leion, T. Mattisson, A. Lyngfelt, Using chemical-looping with oxygen uncoupling (CLOU) for combustion of six different solid fuels, Energy Procedia 1 (1) (2009) 447–453, https://doi.org/10.1016/j.egypro.2009.01.060.
[42] T. Mattisson, A. Lyngfelt, H. Leion, Chemical-looping with oxygen uncoupling for combustion of solid fuels, In. J. Greenh. Gas Control 3 (1) (2009) 11–19, https://doi.org/10.1016/j.ijggc.2008.06.002.
[43] M. Arjmand, H. Leion, T. Mattisson, A. Lyngfelt, Investigation of different manganese ores as oxygen carriers in chemical-looping combustion (CLC) for solid fuels, Appl. Energy 113 (2014) 1883–1894, https://doi.org/10.1016/j.apenergy.2013.06.015.
[44] S. Sundqvist, N. Khalilian, H. Leion, T. Mattisson, A. Lyngfelt, Manganese ores as oxygen carriers for chemical-looping combustion (CLC) and chemical-looping with oxygen uncoupling (CLOU), J. Environ. Chem. Eng. 5 (3) (2017) 2552–2563, https://doi.org/10.1016/j.jece.2017.05.007.
[45] M. Arjmand, H. Leion, A. Lyngfelt, T. Mattisson, Use of manganese ore in chemical-looping combustion (CLC)—effect on steam gasification, In. J. Greenh. Gas Control 8 (2012) 56–60, https://doi.org/10.1016/j.ijggc.2012.02.001.
[46] A. Abad, T. Mattisson, A. Lyngfelt, M. Rydén, Chemical-looping combustion in a 300W continuously operating reactor system using a manganese-based oxygen carrier, Fuel 85 (9) (2006) 1174–1185, https://doi.org/10.1016/j.fuel.2005.11.014.
[47] M. Johansson, T. Mattisson, A. Lyngfelt, Investigation of Mn3O4 with stabilized ZrO2 for chemical-looping combustion, Chem. Eng. Res. Des. 84 (9) (2006) 807–818, https://doi.org/10.1205/cherd.05206.
[48] P. Bartocci, A. Abad, A.C. Flores, M. de las Obras Loscertales, Ilmenite: a promising oxygen carrier for the scale-up of chemical looping, Fuel 337 (2023) 126644, https://doi.org/10.1016/j.fuel.2022.126644.
[49] J.-E. Eriksson, M. Zevenhoven, P. Yrjas, A. Brink, L. Hupa, Corrosion of heat transfer materials by potassium-contaminated ilmenite bed particles in chemical-looping combustion of biomass, Energies 15 (8) (2022) 2740, https://doi.org/10.3390/en15082740.
[50] A. Gyllén, P. Knutsson, F. Lind, H. Thunman, Magnetic separation of ilmenite used as oxygen carrier during combustion of biomass and the effect of ash layer buildup on its activity and mechanical strength, Fuel 269 (2020) 117470, https://doi.org/10.1016/j.fuel.2020.117470.
[51] A. Corcoran, J. Marinkovic, F. Lind, H. Thunman, P. Knutsson, M. Seemann, Ash properties of ilmenite used as bed material for combustion of biomass in a circulating fluidized bed boiler, Energy Fuel 28 (12) (2014) 7672–7679, https://doi.org/10.1021/ef501810u.
[52] I. Staničić, J. Brorsson, A. Hellman, T. Mattisson, R. Backman, Thermodynamic analysis on the fate of ash elements in chemical looping combustion of solid fuels—iron-based oxygen carriers, Energy Fuel 36 (17) (2022) 9648–9659, https://doi.org/10.1021/acs.energyfuels.2c01578.
[53] I. Gogolev, A.H. Soleimanisalim, C. Linderholm, A. Lyngfelt, Commissioning, performance benchmarking, and investigation of alkali emissions in a 10 kWth solid fuel chemical looping combustion pilot, Fuel 287 (2021) 119530, https://doi.org/10.1016/j.fuel.2020.119530.
[54] V. Andersson, A.H. Soleimanisalim, X. Kong, F. Hildor, H. Leion, et al., Alkali-wall interactions in a laboratory-scale reactor for chemical looping combustion studies, Fuel Process. Technol. 217 (2021) 106828, https://doi.org/10.1016/j.fuproc.2021.106828.
[55] V. Andersson, A.H. Soleimanisalim, X. Kong, H. Leion, T. Mattisson, J.B. C. Pettersson, Alkali interactions with a calcium manganite oxygen carrier used in chemical looping combustion, Fuel Process. Technol. 227 (2022) 107099, https://doi.org/10.1016/j.fuproc.2021.107099.
[56] V. Andersson, X. Kong, H. Leion, T. Mattisson, J.B.C. Pettersson, Design and first application of a novel laboratory reactor for alkali studies in chemical looping applications, Fuel Process. Technol. 252 (2023) 107988, https://doi.org/10.1016/j.fuproc.2023.107988.
[57] A.A. Larbi, L. Akil, M. Ahmed, C. Tigani, Experimental measurement of moisture sorption isotherms and isosteric heat of palm hearts (Jomare) harvested in the Algerian Sahara, Instrument. Mesure Metrol. 18 (2019) 297–304, https://doi.org/10.18280/i2m.180310.
[58] M. Hagström, K. Engvall, J.B.C. Pettersson, Desorption kinetics at atmospheric pressure: alkali metal ion emission from hot platinum surfaces, J. Phys. Chem. B 104 (18) (2000) 4457–4462, https://doi.org/10.1021/jp000311w.
[59] U. Jäglid, J.G. Olsson, J.B.C. Pettersson, Detection of sodium and potassium salt particles using surface ionization at atmospheric pressure, J. Aerosol Sci. 27 (6) (1996) 967–977, https://doi.org/10.1016/0021-8502(96)00025-0.
[60] K. Davidsson, K. Engvall, M. Hagström, J. Korsgren, B. Lönn, J. Pettersson, A surface ionization instrument for on-line measurements of alkali metal components in combustion: instrument description and applications, Energy Fuels 16 (2002), https://doi.org/10.1021/ef020020h.
[61] D. Gall, M. Pushp, A. Larsson, K. Davidsson, J.B.C. Pettersson, Online measurements of alkali metals during start-up and operation of an industrial-scale biomass gasification plant, Energy Fuel 32 (1) (2018) 532–541, https://doi.org/10.1021/acs.energyfuels.7b03135.

[62] V. Andersson, Y. Ge, X. Kong, J.B.C. Pettersson, A novel method for on-line characterization of alkali release and thermal stability of materials used in thermochemical conversion processes, Energies 15 (12) (2022) 4365, https://doi.org/10.3390/en15124365.
[63] M. Pushp, D. Gall, K. Davidsson, M. Seemann, J.B.C. Pettersson, Influence of bed material, additives, and operational conditions on alkali metal and tar concentrations in fluidized bed gasification of biomass, Energy Fuel 32 (6) (2018) 6797–6806, https://doi.org/10.1021/acs.energyfuels.8b00159.
[64] D. Gall, J. Viljanen, I. Gogolev, T. Allgurén, K. Andersson, Alkali monitoring of Industrial process gas by surface ionization—calibration, assessment, and comparison to in situ laser diagnostics, Energy Fuel (2021), https://doi.org/10.1021/acs.energyfuels.1c03205.
[65] P. Hallberg, M. Hanning, M. Rydén, T. Mattisson, A. Lyngfelt, Investigation of a calcium manganite as oxygen carrier during 99h of operation of chemical-looping combustion in a 10kWth reactor unit, In. J. Greenh. Gas Control 53 (2016) 222–229, https://doi.org/10.1016/j.ijggc.2016.08.006.
[66] D. Gall, M. Pushp, K.O. Davidsson, J.B.C. Pettersson, Online measurements of alkali and heavy tar components in biomass gasification, Energy Fuel 31 (8) (2017) 8152–8161, https://doi.org/10.1021/acs.energyfuels.7b00474.
[67] W.C. Hinds, Aerosol Technology - Properties, Behavior and Measurement of Airborne Particles, Wiley, New York, 1999.
[68] T. Blomberg, P. Makkonen, M. Hiltunen, Role of alkali hydroxides in the fireside corrosion of heat transfer surfaces, a practical approach, Mater. Sci. Forum 461-464 (2004) 883–890.
[69] M. Zevenhoven, P. Yrjas, M. Hupa, Ash-Forming Matter and Ash-Related Problems, 2010, https://doi.org/10.1002/9783527628148.hoc068.
[70] L. Klopper, C.A. Strydom, J.R. Bunt, Influence of added potassium and sodium carbonates on CO2 reactivity of the char from a demineralized inertinite rich bituminous coal, J. Anal. Appl. Pyrolysis 96 (2012) 188–195, https://doi.org/10.1016/j.jaap.2012.04.005.
[71] S. Ramireddy, B. Zheng, E. Nguyen, Periodic Trends, Chemistry LibreTexts. https://chem.libretexts.org/Bookshelves/Inorganic_Chemistry/Supplemental_Modules_and_Websites_(Inorganic_Chemistry)/Descriptive_Chemistry/Periodic_Trends_of_Elemental_Properties/Periodic_Trends, 2023 (Accessed 09-10 2023).
[72] D.C. Dayton, T.A. Milne, Laboratory measurements of alkali metal containing vapors released during biomass combustion, in: L. Baxter, R. DeSollar (Eds.), Applications of Advanced Technology to Ash-Related Problems in Boilers, Springer US, Boston, MA, 1996, pp. 161–185, https://doi.org/10.1007/978-1-4757-9223-2_11.
[73] C. Li, K.C.K. Soh, P. Wu, Formability of ABO3 perovskites, J. Alloys Compd. 372 (1) (2004) 40–48, https://doi.org/10.1016/j.jallcom.2003.10.017.
[74] M. Rydén, H. Leion, T. Mattisson, A. Lyngfelt, Combined oxides as oxygen-carrier material for chemical-looping with oxygen uncoupling, Appl. Energy 113 (2014) 1924–1932, https://doi.org/10.1016/j.apenergy.2013.06.016.
[75] D. Bhogeswara Rao, M. Rigaud, Kinetics of the oxidation of ilmenite, Oxid. Met. 9 (1) (1975) 99–116, https://doi.org/10.1007/BF00613496.
[76] J. Zhang, Q. Zhu, Z. Xie, C. Lei, H. Li, Morphological changes of panzhihua ilmenite during oxidation treatment, Metall. Mater. Trans. B Process Metall. Mater. Process. Sci. 44 (2013), https://doi.org/10.1007/s11663-013-9863-3.
[77] J. Adánez, A. Cuadrat, A. Abad, P. Gayán, L.F. de Diego, F. García-Labiano, Ilmenite activation during consecutive redox cycles in chemical-looping combustion, Energy Fuel 24 (2) (2010) 1402–1413, https://doi.org/10.1021/ef900856d.
[78] C.W. Bale, E. Bélisle, P. Chartrand, S.A. Decterov, G. Eriksson, et al., FactSage thermochemical software and databases, 2010–2016, Calphad 54 (2016) 35–53, https://doi.org/10.1016/j.calphad.2016.05.002.
[79] S. Link, P. Yrjas, D. Lindberg, A. Trikkel, Characterization of Ash Melting of Reed and Wheat Straw Blend, ACS Omega 7 (2) (2022) 2137–2146, https://doi.org/10.1021/acsomega.1c05087.
[80] A. Cabello, A. Abad, M.T. Izquierdo, P. Gayán, L.F. de Diego, et al., Qualification of operating conditions to extend oxygen carrier utilization in the scaling up of chemical looping processes, Chem. Eng. J. 430 (2022) 132602, https://doi.org/10.1016/j.cej.2021.132602.
[81] W. Wang, R. Lemaire, A. Bensakhria, D. Luart, Review on the catalytic effects of alkali and alkaline earth metals (AAEMs) including sodium, potassium, calcium and magnesium on the pyrolysis of lignocellulosic biomass and on the co-pyrolysis of coal with biomass, J. Anal. Appl. Pyrolysis 163 (2022) 105479, https://doi.org/10.1016/j.jaap.2022.105479.